Biochimica et Biophysica Acta 1837 (2014) 717–725

Contents lists available at ScienceDirect

Biochimica et Biophysica Acta

journal homepage: www.elsevier.com/locate/bbabio

Redox tuning of the catalytic activity of soluble fumarate reductases from *Shewanella*

Catarina M. Paquete, Ivo H. Saraiva, Ricardo O. Louro *

Instituto de Tecnologia Química e Biológica, Universidade Nova de Lisboa, Av. da República — EAN, 2780-157 Oeiras, Portugal

ARTICLE INFO

Article history:
Received 19 December 2013
Received in revised form 4 February 2014
Accepted 6 February 2014
Available online 14 February 2014

Keywords:
Electron transfer
Fumarate reductase
Shewanella
Cytochrome
NMR
Stopped-flow

ABSTRACT

Many enzymes involved in bioenergetic processes contain chains of redox centers that link the protein surface, where interaction with electron donors or acceptors occurs, to a secluded catalytic site. In numerous cases these redox centers can transfer only single electrons even when they are associated to catalytic sites that perform two-electron chemistry. These chains provide no obvious contribution to enhance chemiosmotic energy conservation, and often have more redox centers than those necessary to hold sufficient electrons to sustain one catalytic turnover of the enzyme. To investigate the role of such a redox chain we analyzed the transient kinetics of fumarate reduction by two flavocytochromes c_3 of *Shewanella* species while these enzymes were being reduced by sodium dithionite. These soluble monomeric proteins contain a chain of four hemes that interact with a flavin adenine dinucleotide (FAD) catalytic center that performs the obligatory two electron–two proton reduction of fumarate to succinate. Our results enabled us to parse the kinetic contribution of each heme towards electron uptake and conduction to the catalytic center, and to determine that the rate of fumarate reduction is modulated by the redox stage of the enzyme, which is defined by the number of reduced centers. In both enzymes the catalytically most competent redox stages are those least prevalent in a quasi-stationary condition of turnover. Furthermore, the electron distribution among the redox centers during turnover suggested how these enzymes can play a role in the switch between respiration of solid and soluble terminal electron acceptors in the anaerobic bioenergetic metabolism of *Shewanella*.

1. Introduction

Protein mediated electron transfer is a ubiquitous process in living organisms. Some of the most relevant examples occur in respiration and photosynthesis where the electron transfer reactions are often coupled to charge translocation. In several cases the catalytic site is buried inside the protein and electrical contact with the protein surface is established by chains of redox centers. Two notable examples are complex I and complex II of the mitochondrial respiratory apparatus where the site of NADH or succinate oxidation, respectively, are connected to the quinone reduction site in the transmembrane region by subunits peripheral to the membrane that contain a chain of iron sulfur clusters [1,2]. The physiological role of these chains of redox centers is not clear: they do not contribute to enhance the transmembrane energy conservation; they are made up of centers that can only perform single electron transfer reactions, even though they are often connected to catalytic sites that perform two-electron chemistry; and they do not serve as temporary electron storage since the number of redox cofactors in these chains often do not match those needed for sustaining one catalytic turnover. The presence of chains of redox centers with those characteristics is not restricted to membrane bound bioenergetic enzymes. A similar situation can also be observed, for example, in soluble hydrogenases where the catalytic center is linked to the protein surface by a chain of iron sulfur clusters [3], in the cytochrome *c* nitrite reductase where a chain of four hemes connects the surface of the protein to the catalytic heme [4], and in soluble flavocytochrome c_3 fumarate reductase (Fcc_3) from *Shewanella* where four hemes link the catalytic center to the protein surface.

The fact that the chain of redox centers is retained in soluble and membrane bound bioenergetic enzymes strongly hints to an essential role played by this feature. Moreover, mutations that affect these redox cofactors were shown to modulate the catalytic activity of these proteins without disturbing the redox properties of their active sites [5,6].

Fcc_3 is one of the most abundant proteins in the periplasmic space of *Shewanella* when this organism is grown anaerobically [7], and is the only functional fumarate reductase in this organism [8,9]. It catalyzes the 'unidirectional' reduction of fumarate to succinate, which is an obligatory two-electron, two-proton process. Recently, it was proposed that Fcc_3 could also participate in the reduction of insoluble iron compounds outside the cell, by interacting with the periplasmic decaheme

Abbreviations: Fcc_3, Flavocytochrome c_3; NMR, Nuclear magnetic resonance; FAD, Flavin adenine dinucleotide

* Corresponding author. Tel.: +351 214469309; fax: +351 214411277.
E-mail address: louro@itqb.unl.pt (R.O. Louro).

http://dx.doi.org/10.1016/j.bbabio.2014.02.006
0005-2728/

cytochrome MtrA [10]. Therefore, it can be classified as a 'moonlighting' protein, which is a protein with more than one function [11]. The molecular structure of Fcc$_3$ reveals that it folds in three domains: the N-terminal domain that contains four *c*-type heme groups and is homologous to the soluble small tetraheme cytochrome of the same organism; the C-terminal domain that is homologous to a flavoprotein subunit of membrane bound fumarate reductases and succinate dehydrogenases, which contains a non-covalently bound flavin adenine dinucleotide group (FAD) where the fumarate reduction occurs; and the clamp domain that links the two previous domains. It was shown that the clamp domain presents a closed conformation in the presence of a ligand and an open conformation in the substrate free enzyme [12,13]. In the N-terminal domain, three of the hemes (I, II and III, numbered according to the order of their attachment to the polypeptide chain) display substantial exposure at the protein surface and therefore may receive electrons from electron donors. Heme IV is buried inside the protein close to the FAD group and is responsible for the electron transfer to the catalytic site [14]. The quasi-linear architecture of the four hemes with short pair-wise distances allows the fast conduction of electrons across the length of the N-terminal domain [12,13] to the active site of the protein. Indeed, NMR data collected for two Fcc$_3$ showed that these proteins display fast intramolecular electron equilibrium allowing an efficient conduction of electrons to the active site [15]. However, the mechanism by which Fcc$_3$ receives the electrons from its physiological electron donor, the membrane-bound tetraheme cytochrome CymA, and efficiently transfers them to either the catalytic active site for the reduction of fumarate, or to MtrA for the reduction of insoluble solid compounds remains to be elucidated. Toward this end, a kinetic characterization of the individual redox centers of Fcc$_3$ from *Shewanella oneidensis* MR-1 and *Shewanella frigidimarina* NCIMB400 as they receive electrons from an electron donor and transfer them during the course of fumarate reduction was performed. The results reveal how the intrinsic properties of this moonlighting enzyme enable the transition between the enzymatic and electron transfer activity, according to the bioenergetic needs of *Shewanella*.

2. Materials and methods

2.1. Protein production

Flavocytochromes c_3 were purified from the soluble fraction of *Shewanella* as previously described for *S. oneidensis* MR-1 [16] and *S. frigidimarina* NCIMB400 [17]. Stock solutions of Fcc$_3$ from both strains were deaerated with cycles of argon and vacuum. Dilutions of the proteins to the desired concentration were made in 100 mM Tris buffer at various pH values. The concentration of the protein was determined by UV–visible spectroscopy using ε_{552nm} of 120,000 M^{-1} cm^{-1} for the reduced state. All manipulations of the samples were performed inside an anaerobic chamber (M-Braun 150) containing less than 10 ppm oxygen.

Precipitation with ammonium sulfate at acid pH was used to remove the FAD group from Fcc$_3$ as described in the literature [18]. The FAD content of Fcc$_3$ was determined by visible spectroscopy using ε_{450nm} of 11,300 M^{-1} cm^{-1} [19].

2.2. NMR binding experiments

Fcc$_3$ from *S. oneidensis* MR-1 and *S. frigidimarina* NCIMB400 were prepared in 20 mM phosphate buffer at pH 7.6 with the ionic strength set by the addition of 100 mM KCl with a concentration of protein between 100 and 200 μM. Stepwise additions of 10 mM solutions of fumarate or succinate were used to observe chemical shift perturbations of the heme signals upon binding. These were measured using 1D NMR experiments performed in a Bruker Avance 500 spectrometer at 25 °C.

2.3. Kinetic experiments

Kinetic data were obtained by measuring the light absorption changes at 552 nm using a stopped-flow spectrometer (SHU-61VX2 from TgK Scientific) placed inside the anaerobic chamber. At this wavelength the hemes display an intense absorption band in the reduced state. The temperature during the kinetic experiments was kept at 298 ± 1 K using an external circulating bath.

2.3.1. Reduction of Fcc$_3$ with sodium dithionite

Sodium dithionite was used to reduce Fcc$_3$. This strong reducing agent was used in large excess to guarantee pseudo-first order conditions facilitating the analysis of the kinetic data [20,21]. Solid sodium dithionite was added to degassed 5 mM Tris buffer at pH 8.0 at a final ionic strength of 100 mM set by the addition of KCl. The concentration of sodium dithionite was determined in each experiment using ε_{314nm} of 8000 M^{-1} cm^{-1} [22]. The reference value for the absorbance of the fully oxidized state of the protein was obtained at 552 nm in the beginning of each experiment by mixing the protein with degassed buffer, while the reference value of the fully reduced state was obtained from the final absorbance taken at effectively infinite time.

Partially reduced protein was prepared by the addition of small amounts of concentrated sodium dithionite solution to give the desired degree of reduction, before initiating the kinetic experiment. At least 1 min elapsed between sample preparations and loading in the stopped flow apparatus for data collection.

The reducing agent was found to be the one-electron donor bisulfite radical (SO_2•) for both proteins, determined according to the work of Lambeth and Palmer [23]. The pH of the samples was confirmed after each kinetic experiment.

2.3.2. Reduction of Fcc$_3$ with sodium dithionite in the presence of fumarate

The reduction of Fcc$_3$ from both *Shewanella* strains was also studied in the presence of fumarate. Fumaric acid was added to the oxidized protein prepared in 100 mM Tris buffer at pH 8.0 in order to have a concentration of 50 μM after mixing. This concentration is above the K_m of 2.5–6 μM reported for Fcc$_3$ from *S. frigidimarina* NCIMB400 based on transient kinetic measurements [24]. Kinetic traces were acquired by mixing this solution with sodium dithionite as described above. The optical density of the protein in the fully oxidized state and fully reduced states were determined as indicated above.

2.3.3. Kinetic models

The experimental data were fitted with kinetic models derived from that previously developed for the discrimination of the contribution of individual hemes towards the reduction of multiheme cytochromes [20]. The detailed population scheme that describes a protein with four hemes and a redox-linked acid–base center contains 16 deprotonated microstates and 16 protonated microstates (Fig. 1A) [21]. NMR data show for both flavocytochromes fast intramolecular electron exchange (>10^5 s^{-1}) and slow intermolecular electron exchange (<10^3 s^{-1}) [15]. This means that during reduction there is intramolecular equilibration of each electron according to the reduction potentials of the redox centers in the protein. Considering the representation of Figs. 1 and 2, there is fast electron exchange within each column that represents a redox stage, and slow exchange across columns. In this situation each electron transfer step is characterized by a macroscopic rate constant (K_{1-4} in Fig. 1A, and K'_{1-6} in Fig. 2) that is given by the weighted average of the individual rate constants (k_i^j) of all the microsteps that participate in that macroscopic step [20]:

$$K = \sum \left(k_i^j \times \chi_i^j \right). \quad (1)$$

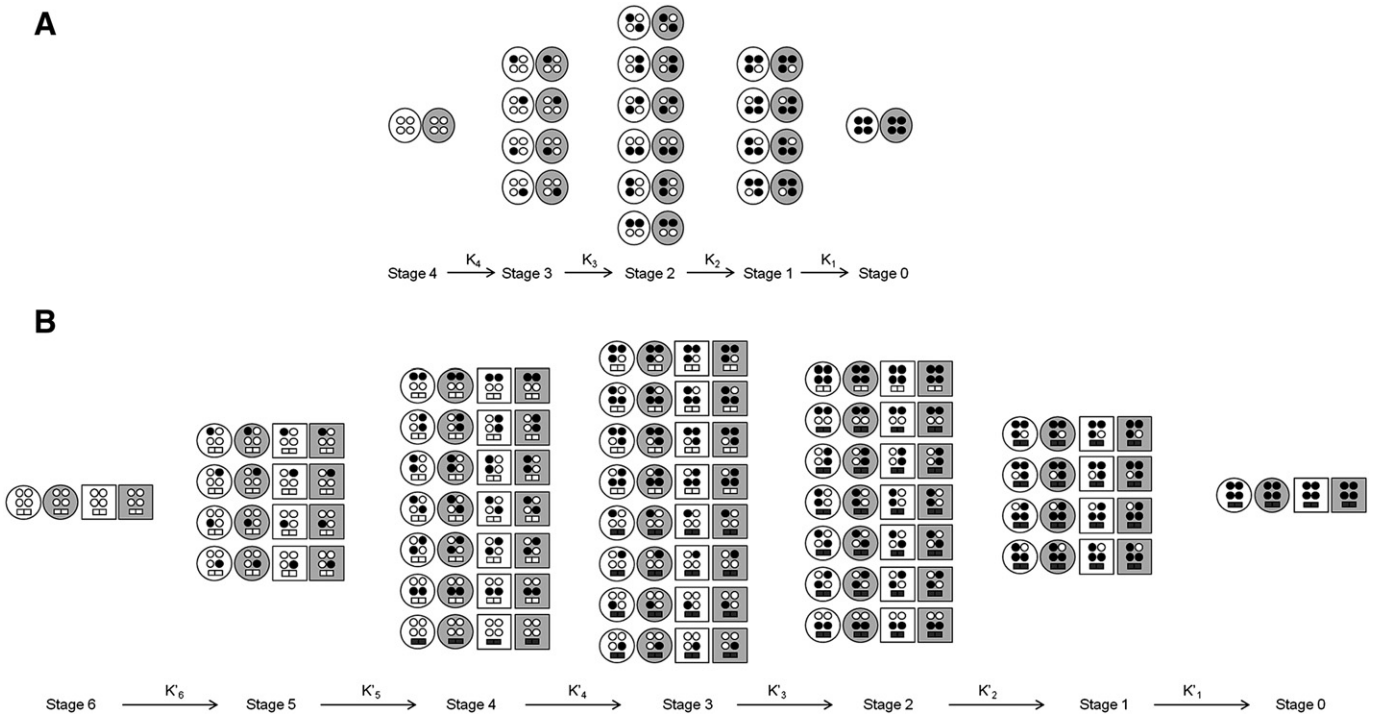

Fig. 1. Schematic representation of the microstates of (A) a protein with four single-electron redox centers (hemes) and one acid–base center; and (B) a protein with four single-electron redox centers (hemes), one two-electron redox center (FAD), and two acid–base redox centers, one affecting the redox properties of the hemes and the other affecting the redox properties of the FAD. The protein is represented as large circles and squares, with circles representing the deprotonated state of the acid–base center associated with the FAD group, and squares representing the protonated state. White and gray protein represents the deprotonated and protonated microstates for the acid–base center associated with the hemes. Black dots and squares represent reduced redox centers, hemes and FAD, respectively. Redox stages are numbered according to the number of electron vacancies in the redox centers of the protein and organized in columns that group populations in fast intramolecular equilibrium with the same number of electrons. Macroscopic electron transfer steps between stages are shown in the direction of reduction and macroscopic rate constants are represented by K_{1-4} in A and K'_{1-6} in B.

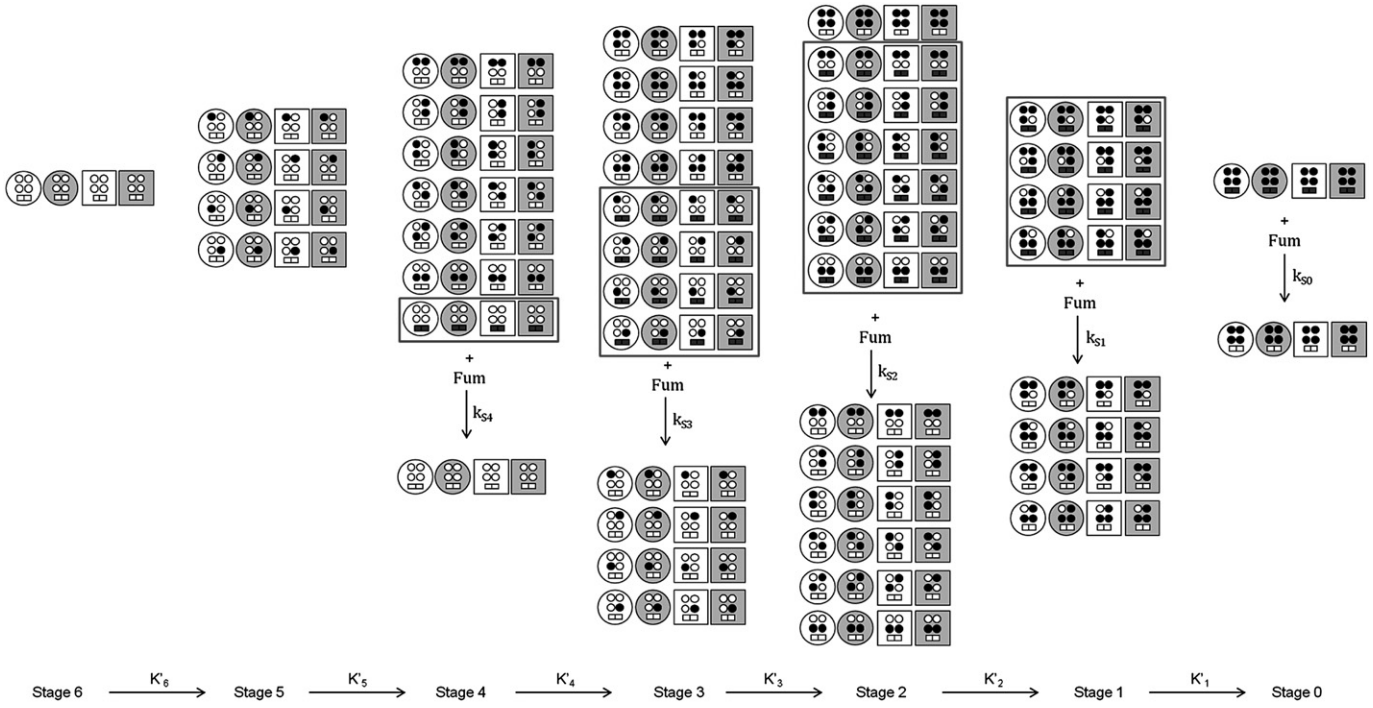

Fig. 2. Population scheme of Fcc_3 when reducing fumarate to succinate in the presence of excess reducing agent. The protein is fully oxidized in stage 6 and fully reduced in stage 0. When at least two electrons are available in Fcc_3, FAD can be reduced by fast intramolecular electron exchange, and the electrons consumed to reduce fumarate. Within each stage, those states that are competent for fumarate reduction are enclosed in boxes. The macroscopic rate constants of electron transfer are defined by K'_{1-6}, whereas the kinetic rate constants for catalysis are defined by k_{S0-S4}, one for each redox stage that contains reduced FAD (stages 4 to 0).

The weighting factors are the relative thermodynamic equilibrium populations of the starting states (χ_i^j). These are known from the thermodynamic properties of these proteins [15]. Each microscopic rate constant is parsed into a reference rate constant (k_i^0), one for each redox center, and an exponential factor that accounts for the driving force of the reaction, as given by Marcus' theory [25]:

$$k_i^j = k_i^0 \exp\left[\frac{e_i^j F}{2RT}\left(1 + \frac{e_D F}{\lambda_{ET}} - \frac{e_i^j F}{2\lambda_{ET}}\right)\right]. \quad (2)$$

Here k_i^0 is the reference rate constant to be calculated, e_i^j is the reduction potential of the heme that is being reduced and is known from the thermodynamic properties of the hemes (Table S1); e_D is the reduction potential of the electron donor [26]; and λ_{ET} is the reorganization energy, which was taken as 1 eV [27] and assumed to be equal for all redox centers and does not change during the reduction process [20,21].

For the case of Fcc$_3$ this scheme has to be expanded to account for the redox and acid–base transitions of the FAD group (Fig. 1B). Since the semiquinone state of the FAD group has never been observed experimentally for *Shewanella* fumarate reductases [28], this state was not included in the model. Therefore, the reduction of the FAD group by the heme domain can only occur when at least two electrons are available in the protein. As a result, the complete population diagram that describes Fcc$_3$ comprises 128 microstates, 64 microstates for the deprotonated condition of the FAD group and 64 microstates for the protonated condition (Fig. 1B).

In the presence of fumarate, two electrons and two protons from the catalytic center are consumed for the reduction to succinate [12,13,28]. Therefore, the population diagram that describes the reduction of Fcc$_3$ in the presence of fumarate involves the extension of the scheme in Fig. 1B to include the catalytic event (Fig. 2).

2.3.4. Kinetic analysis

Data obtained for the reduction of Fcc$_3$ from *S. oneidensis* MR-1 and *S. frigidimarina* NCIMB400 with sodium dithionite were normalized to have oxidized fraction *versus* time, and the timescale was corrected for the dead time of the apparatus according to the manufacturer's instructions. A minimum of two data sets for each experimental condition were averaged to reduce electrical noise.

The thermodynamic properties of the heme domain of both proteins which includes the reduction potential of each heme, the pK_a of the acid–base center as well as the redox and redox-Bohr interactions between hemes and between hemes and the acid–base center were obtained from the work of Pessanha et al. (Table S1) [15]. The reduction potential of the FAD group and its pK_a were taken from the work of Turner et al. [28]. Due to the similar environment of the catalytic domain in both *Shewanella* Fcc$_3$ it was assumed that the potentials and pH dependence of the FAD measured for *S. frigidimarina* NCIMB400 [28] are similar for the Fcc$_3$ from *S. oneidensis* MR-1. The close proximity of the FAD group to heme IV in Fcc$_3$ leads to an anti-cooperative redox interaction between these two centers, which was estimated to be approximately 10 mV based on the distance (~7 Å for closest atoms) [29].

The experimental data obtained for the reduction of each protein with sodium dithionite in the absence of fumarate at various pH values were fitted simultaneously using the model in Fig. 1, while the experimental data obtained for the reduction of each flavocytochrome in the presence of fumarate were fitted using the model in Fig. 2. The analysis of the reduction of Fcc$_3$ in the presence of fumarate was performed considering that the contribution of each heme toward the reduction of the protein by sodium dithionite is the same as in the absence of the substrate, which is supported by the structural organization of the protein in three domains [12]. The kinetic models were implemented in Matlab and fit to the experimental data using the Nelder–Mead algorithm [30]. The m-file is available upon request.

3. Results

3.1. Protein production and characterization

Fcc$_3$ from *S. oneidensis* MR-1 and *S. frigidimarina* NCIMB400 were considered to be pure by the observation of a single band in SDS-PAGE and an absorbance ratio $A_{Soret\ Peak}/A_{280nm}$ higher than 4.5 [16]. Given that in these fumarate reductases the FAD group is not covalently bound, the FAD content was determined, revealing 83% and 90% holoprotein in the samples of Fcc$_3$ from *S. oneidensis* MR-1 and *S. frigidimarina* NCIMB400, respectively. These data were used in the kinetic analysis to account for the fraction of Fcc$_3$ without FAD, which is not catalytically competent in fumarate reduction but is still redox active.

3.2. Determination of the electron entry point when Fcc$_3$ is reduced by sodium dithionite

Protein film voltammetry revealed direct reduction of the FAD group independent of the heme domain [31], which shows that reduction of Fcc$_3$ *in vitro* can proceed *via* two different routes: the electrons can be uptaken by the hemes, or by the FAD group. To investigate which of these routes is more important, holo-Fcc$_3$ and Fcc$_3$ deliberately stripped of the FAD were reacted with sodium dithionite and the reduction of the hemes was followed spectroscopically at 552 nm. The data revealed similar reduction kinetics of the hemes in both proteins, indicating that, in the holoprotein, the intramolecular equilibrium between the FAD and the hemes does not disturb the reduction of the hemes (Fig. 3). This is likely a consequence of the fast direct reduction of FAD by sodium dithionite. FAD has the most positive reduction potential, which makes it the easiest redox center of Fcc$_3$ to be reduced, becoming unavailable to receive electrons from the hemes. Otherwise, the fast intramolecular electron equilibrium between the redox centers would drain the first two electrons captured by the hemes to the FAD, leading to the observation of a lag phase in the kinetic trace of reduction of the hemes.

3.3. Determination of the reference rate constants for reduction of each heme by sodium dithionite

The data of Fcc$_3$ reduction with sodium dithionite were collected starting with Fcc$_3$ fully oxidized or pre-equilibrated at partial degrees of reduction. The slow intermolecular equilibrium makes the populations of microscopic states in the starting condition of samples partially

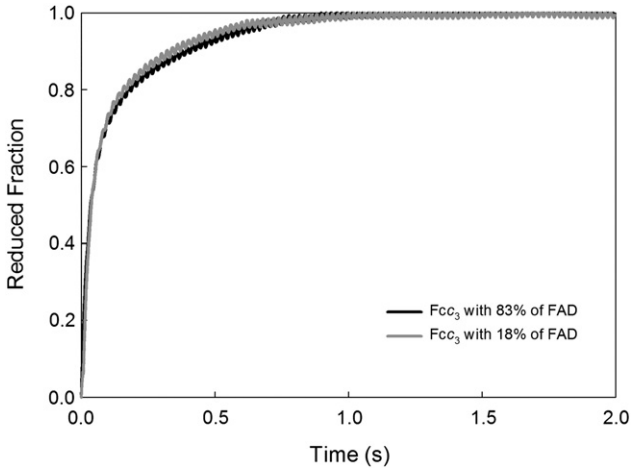

Fig. 3. Kinetics of reduction of Fcc$_3$ from *S. oneidensis* MR-1 with 83% of FAD (A) and with 18% of FAD (B) by sodium dithionite at pH 7.7. The concentration of sodium dithionite was 108 μM and the concentration of Fcc$_3$ from *S. oneidensis* MR-1 with 83% of FAD and with 18% of FAD was 0.80 and 0.92 μM respectively.

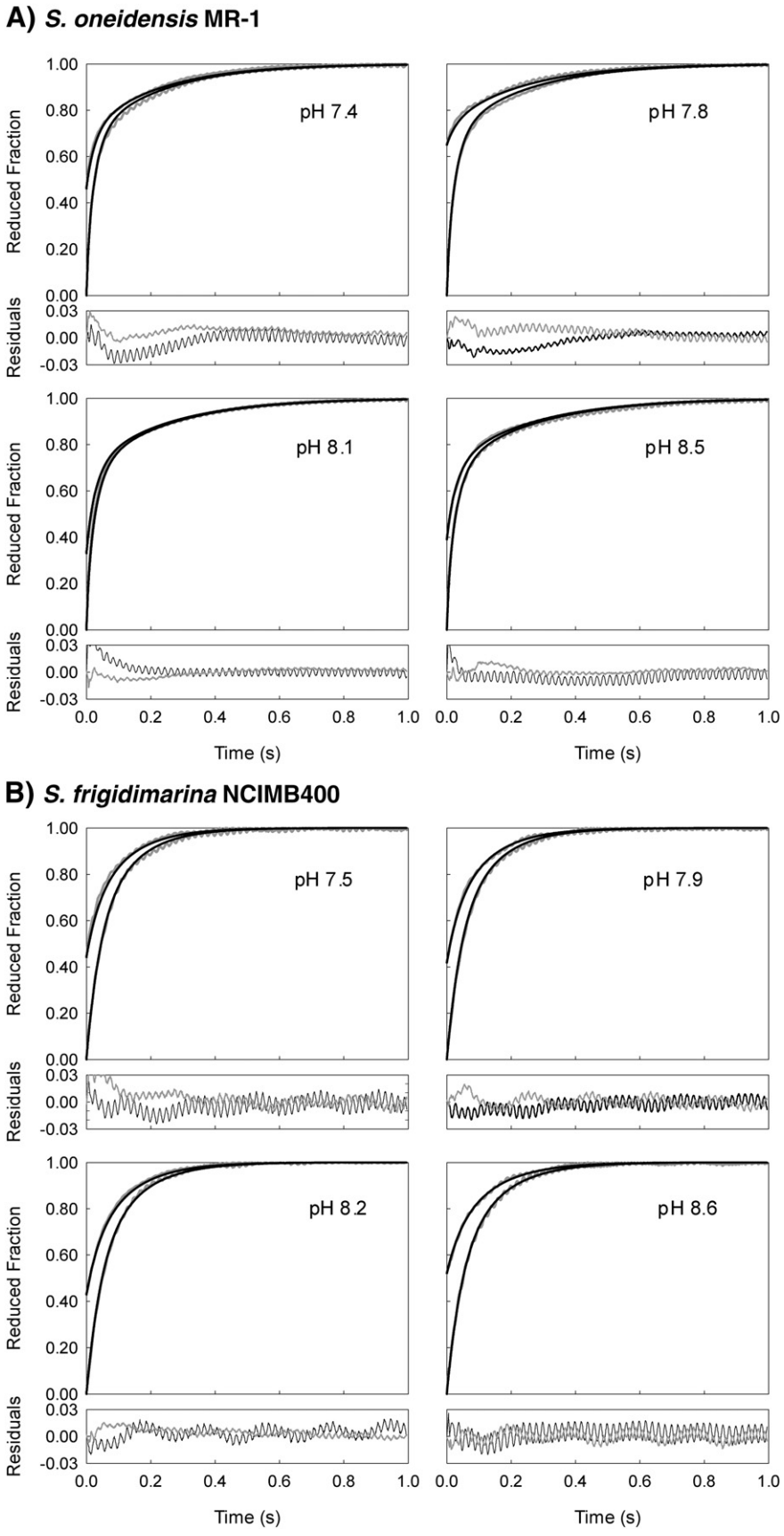

Fig. 4. Kinetic traces of reduction of Fcc_3 from *S. oneidensis* MR-1 (A) and *S. frigidimarina* NCIMB400 (B) by sodium dithionite at various pH values. The gray lines are the kinetic data and black lines are the simultaneous fit of the kinetic model to data obtained at the four pH values and different initial degrees of oxidation. The concentration of sodium dithionite was 118 μM and 53 μM for Fcc_3 from *S. oneidensis* MR-1 and *S. frigidimarina* NCIMB400 respectively. The concentration of Fcc_3 from *S. oneidensis* MR-1 was approximately 0.8 μM, and approximately 0.6 μM for *S. frigidimarina* NCIMB400. The residuals of the fit are presented, with the range of the magnified vertical scale equal to the magnitude of the experimental uncertainty considered in the fit.

oxidized different from those found at the same level of oxidation when the protein starts from the fully oxidized state. Given that in our experimental conditions the reduction of the heme domain is independent of the FAD group, the data obtained at four pH values spanning the physiological range reported in Fig. 4 were fitted simultaneously with model A of Fig. 1. The resulting four reference rate constants, one for each heme in Fcc_3, are reported in Table 1. These constants are independent of the effects of driving force and intrinsic to each individual heme, accounting for structural factors of the heme environment [20].

The data show that the reduction of Fcc_3 with sodium dithionite is not influenced significantly by pH within the range tested. For both proteins the electrons enter through hemes I and II, and are subsequently distributed among the hemes by fast intramolecular electron exchange according to their reduction potentials. Hemes III and VI with reference rate constants several orders of magnitude lower, provide no significant contribution to the uptake of electrons by either cytochrome.

3.4. Effect of fumarate on the accessibility of sodium dithionite to the FAD center

The data reported in Fig. 6 reveal that when fumarate is present, the reduction of the hemes in Fcc_3 with sodium dithionite occurs in a protracted manner. These data show that the catalytic activity of fumarate reduction relies on the drainage of electrons from the heme domain to the FAD. Otherwise, if direct reduction of FAD by sodium dithionite occurred at a rate commensurate with the rate of reduction of the hemes, fumarate reduction could take place without draining electrons from the heme domain, and the kinetic traces of heme reduction would be identical to those obtained in the absence of fumarate. These observations lead us to conclude that, in the presence of fumarate, direct reduction of FAD must be slower than the intramolecular re-equilibration of the electrons received by the hemes.

The slower access of sodium dithionite to the FAD in the presence of fumarate can be a consequence of the conformational modification that occurs upon substrate binding [13], a consequence of the steric bulk of fumarate preventing access of dithionite to the FAD, or even a combination of both factors. The X-ray structures show that binding of the hydrated malate-like molecule in the active site of Fcc_3 did not lead to structural changes in the heme domain [12,13]. Nevertheless, binding of fumarate and succinate to both Fcc_3 in the oxidized state, disturbed the NMR signals of the methyls of all hemes except heme I, which is further away from the binding site. These changes reveal that ligand binding induces dynamic fluctuations in the structure with interconversion faster than 50 s^{-1}. For the case of Fcc_3 from *S. oneidensis* MR-1, observation of signals in fast and slow exchanges in the NMR time scale confined the rate of interconversion between 50 and 250 s^{-1} (Fig. 5). However, all signals are disturbed less than 0.5 ppm, which is compatible with the lack of significant changes in the crystal structure.

3.5. Determination of the contribution of each redox stage towards fumarate reduction

Given the evidence for small conformational changes in the heme domain, the reduction potentials and interactions reported in the literature (Table S1) [15] together with the intrinsic kinetic rate constants reported in Table 1 were used as input in the model of Fig. 2. The fast intramolecular electron exchange between all the redox centers [15,32] ensures that the population distribution within each stage can be known from the thermodynamic properties of the proteins, and once a minimum of two electrons are available in Fcc_3, fumarate can be reduced. This catalytic event consumes two electrons and two protons from the active site in the presence of fumarate. Only stages V and VI that are made of populations containing one and zero electrons, respectively, are not competent for fumarate reduction due to the lack of sufficient electrons in the enzyme. The results of fitting this model to the kinetic data obtained for both Fcc_3 are shown in Fig. 6, giving the 5 macroscopic rate constants for fumarate reduction presented in Table 2, which are well defined by the data as can be appreciated by the magnitude of the respective standard errors.

Table 1
Reference rate constants for the reduction of each heme in Fcc_3 from *S. oneidensis* MR-1 and *S. frigidimarina* NCIMB400 at 25 °C.

	k_i^0 ($\times 10^9$ s^{-1} M^{-1})			
	Heme I	Heme II	Heme III	Heme IV
S. oneidensis MR-1	2.34 (0.09)	1.36 (0.05)	0.00 (0.11)	0.00 (0.10)
S. frigidimarina NCIMB400	1.93 (0.06)	2.77 (0.07)	0.00 (0.08)	0.00 (0.07)

Standard errors, shown in parenthesis, were obtained from the diagonal elements of the covariance matrix considering an experimental uncertainty of 5% of the total amplitude of the optical signal in the kinetic traces.

4. Discussion

The soluble monomeric nature of Fcc_3 and its moderate size (64 kDa) when compared with membrane associated fumarate reductases facilitated its detailed thermodynamic characterization [15]. This characterization was used in this work to define the populations of each heme in the electron transfer events that take place in the heme redox chain during catalysis.

In the absence of fumarate, both the heme and FAD domains of Fcc_3 are directly reduced by the reducing agent. As a result this electron transfer does not occur to a significant extent during the period required for the reduction of the hemes by sodium dithionite. This is despite the short distance between heme IV and the FAD group (less than 7.5 A ring to ring) that makes intramolecular electron exchange between the two groups fast and not rate limiting [15]. For both flavocytochromes, the reduction of the heme domain by sodium dithionite occurs through hemes I and II. In both proteins heme II has the lowest reduction potential but considerable solvent exposure [12,13,15]. Thus, the more negative reduction potential of this heme ensures that once the electrons enter the protein, the redistribution among the other hemes according to their reduction potentials is a spontaneous process. This leaves heme II available to receive further electrons from a donor of multiple electrons such as the physiological partner CymA. Further support for this proposal comes from the observation that the NMR signals of heme II are the most disturbed in docking studies of Fcc_3 from *S. oneidensis* MR-1 with the physiological partners MtrA and CymA [16]. Given that hemes I and II of Fcc_3 are adjacent, closely spaced and well exposed on the surface of Fcc_3, the available experimental data indicate that interaction between Fcc_3 and CymA involves the same surface region as that probed by dithionite.

The oxidation of the heme domain by fumarate is a complex process with biphasic kinetics for the change in absorbance of the hemes [17]. Our analysis sheds light on this process by parsing the contribution of each catalytically competent redox stage of the enzymes. The observation that different redox stages of the enzymes display different catalytic rates has to be reconciled with the well established data on solvent kinetic isotope effect that reveals proton transfer to be the rate limiting process [5,32]. Given that the hemes have negligible pH dependence of the reduction potentials in the physiological pH range (redox-Bohr effect) the coupling between the redox stage and the catalytic efficiency cannot be thermodynamic. Our NMR data reveal the appearance of dynamic conformational fluctuations upon binding of fumarate or succinate to the fully oxidized enzyme. Given that it is known from Fcc_3 mutants that these conformational changes do not affect the access of substrate or product release but affect catalysis [33], a change in the rate of these conformational fluctuations depending on the oxidation stage can provide the dynamic link between the redox stages and the catalytic efficiency of Fcc_3. Such mechanism is similar to that reported for the dihydrofolate reductase from *Escherichia coli*, where perturbations

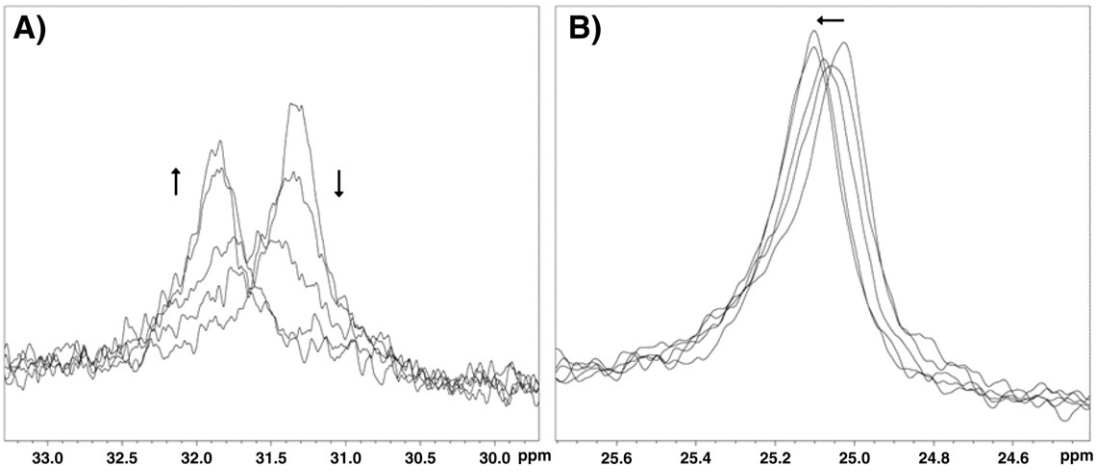

Fig. 5. Changes in NMR signals from two methyls of heme III of Fcc_3 from *S. oneidensis* MR-1 illustrating slow- (A) and fast-exchanges (B) in the NMR time scale at 500 MHz and 25 °C, upon binding of fumarate. Arrows indicate the changes arising from increasing amounts of fumarate.

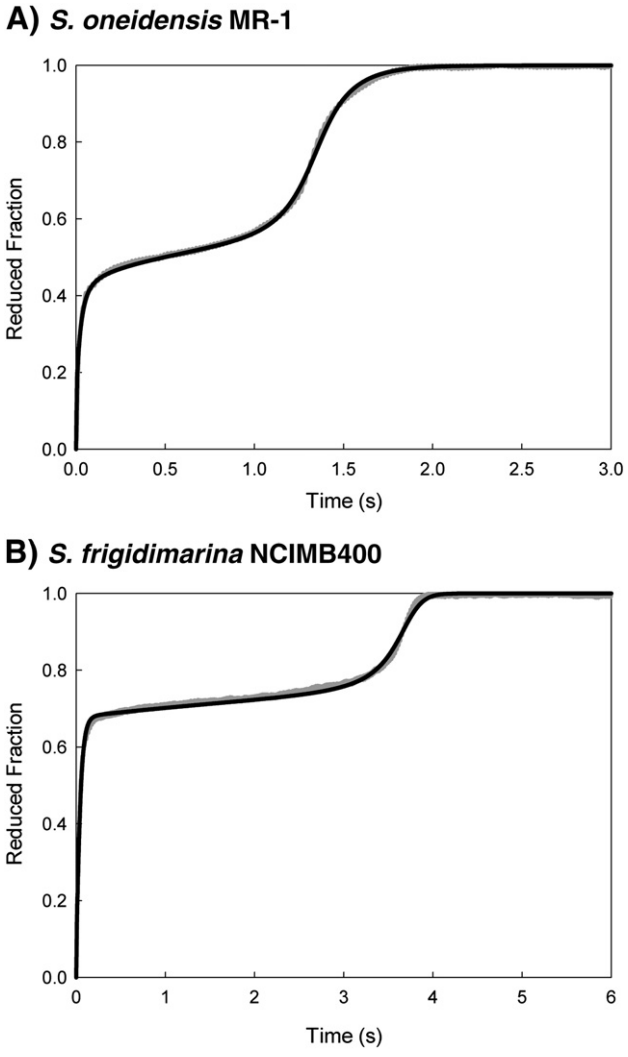

Fig. 6. Kinetic traces of reduction of Fcc_3 from *S. oneidensis* MR-1 (A) and *S. frigidimarina* NCIMB400 (B) by sodium dithionite in the presence of 50 μM fumarate at pH 8.1. The gray lines are the kinetic data and black lines are the fit of the kinetic model to the data. The concentration of sodium dithionite was 331 μM for both Fcc_3, and the concentration of protein was 1.2 μM for Fcc_3 from *S. oneidensis* MR-1 and 1 μM for Fcc_3 from *S. frigidimarina* NCIMB400.

in conformational fluctuations in the millisecond time-scale affect its chemical step of catalysis [34].

Our data reveal that the fastest reduction of fumarate occurs for stage 0 in the case of Fcc_3 from *S. frigidimarina* NCIMB400, and stage 1 for Fcc_3 from *S. oneidensis* MR-1. As a consequence, during fumarate reduction the electrons are efficiently drained from the heme domain of *S. oneidensis* MR-1 Fcc_3 at an earlier stage than in the case of Fcc_3 from *S. frigidimarina* NCIMB400. This gives origin to the different reduction fraction observed in Fig. 6 for the two proteins while fumarate is being reduced. Preliminary data indicates that the initial amount of fumarate in the sample determines the duration of the period during which the Fcc_3 are held in a partially reduced condition, but does not affect the degree of reduction at which the enzyme is held until fumarate is exhausted from the sample. Approximately 50% of the heme domain is reduced in Fcc_3 from *S. oneidensis* MR-1, whereas more than 70% of the heme domain is reduced for *S. frigidimarina* NCIMB400 Fcc_3. The difference in the overall extent of reduction of the proteins during catalysis translates into differences in the prevalence of the individual redox stages (Fig. 7).

The observation of Fig. 7 bearing in mind the results reported in Table 2 shows that the redox stages that reach higher prevalence during catalysis while the protein is being reduced are those that display the slowest kinetic rate for fumarate reduction. This reveals that the most prevalent stages during turnover are those least important for catalysis, and that is the reason for their accumulation to a greater extent as catalysis is taking place. While in *S. frigidimarina* NCIMB400 Fcc_3 accumulates in stage 1, in Fcc_3 from *S. oneidensis* MR-1 it is stage 2 that presents the slowest rate constant for fumarate reduction and is the predominant stage in Fig. 7. The stages that are catalytically more active have a small population because of continuous depletion by the substrate. This information is of crucial importance for the analysis of bioenergetic

Table 2
Kinetic rate constants for the reduction of fumarate at pH 8.1 by Fcc_3 from *S. oneidensis* MR-1 and *S. frigidimarina* NCIMB400.

$\times 10^5$ (M^{-1} s^{-1})	*S. oneidensis* MR-1	*S. frigidimarina* NCIMB400
k_{S4}	92.5 (11.0)	3.2 (4.2)
k_{S3}	8.3 (7.0)	27.0 (3.1)
k_{S2}	0.0 (2.9)	0.2 (4.4)
k_{S1}	301.7 (10.6)	0.9 (1.9)
k_{S0}	17.0 (12.0)	148.3 (9.5)

Standard errors, shown in parenthesis, were calculated from the diagonal elements of the covariance matrix considering an experimental uncertainty of 5% of the total amplitude of the optical signal in the kinetic traces.

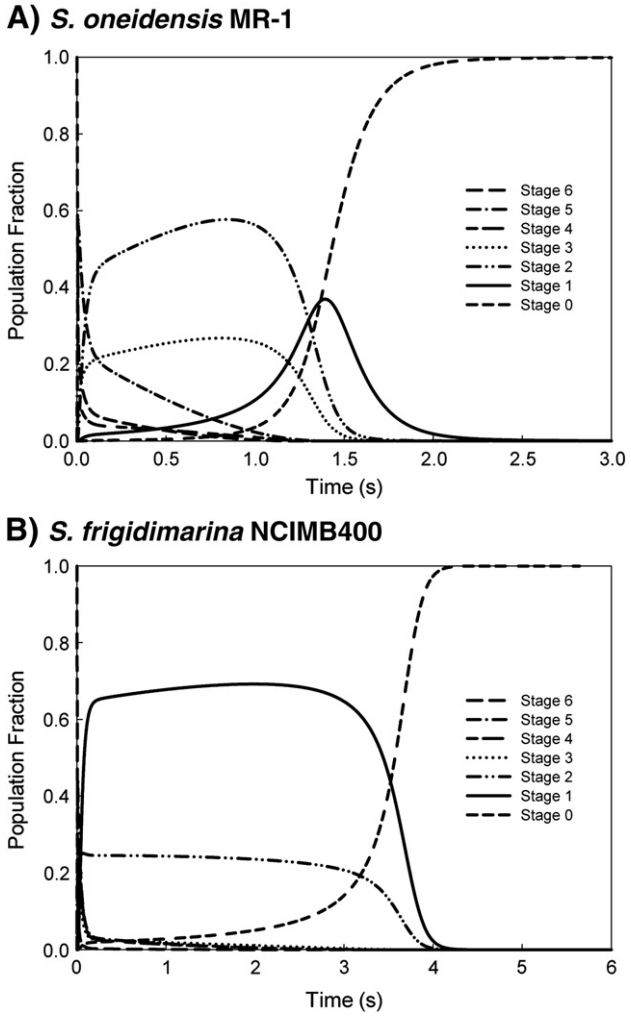

Fig. 7. Reduced fraction of the various redox stages during the reduction of Fcc_3 from *S. oneidensis* MR-1 (A) and *S. frigidimarina* NCIMB400 (B) with sodium dithionite in the presence of fumarate at pH 8.1 and pH 8.2 respectively. The population fractions were obtained using the thermodynamic properties of both Fcc_3 [15] (Table S1), the reference rate constants of Table 1, and the kinetic rate constants for fumarate reduction presented in Table 2.

proteins in general, suggesting that the redox stages that can be observed in significant abundance during turnover may not be those relevant for understanding the catalytic mechanism of the particular enzyme under study. Moreover, the identification of stages 0 and 1 as kinetically competent is relevant for the catalytic bias of these redox enzymes towards fumarate reduction *versus* succinate oxidation. The causes of catalytic bias have been assigned to different rate limiting steps in the two directions of activity [35]. Our data agree with this interpretation, given that the most efficient stages for fumarate reduction are not competent for succinate oxidation, since they cannot accept the two electrons resulting from the reaction.

5. Conclusion

Parsing the kinetic contribution of each heme of two Fcc_3 enabled the discrimination, at the microscopic level, of how these enzymes receive electrons from the donor and feed them to the active site for catalysis. It showed that the catalytic activity is enhanced in the later stages of reduction, which establishes a molecular rationale for the proposal of moonlighting activity for Fcc_3 *in vivo* [10], that matches its apparent origin from the tetraheme cytochrome module and the flavoprotein module joined by a clamp domain. Indeed, the properties of Fcc_3 reveal similarities to those of electronic transistors. At low electron flux from the cell metabolism, or with high availability of solid terminal electron acceptors, Fcc_3 will not charge up to a significant extent from CymA and will transfer the electrons to the outer membrane reductases for the reduction of solid phase acceptors [10,16]. As the electron flux increases, or extracellular electron acceptors become scarce, Fcc_3 will become increasingly reduced, switching to efficient catalysis of fumarate reduction. This switching mechanism can be crucial to prevent metabolic arrest and allow *Shewanella* to quickly alternate between reduction of soluble and insoluble electron acceptors, bypassing transcriptional regulation [36].

Supplementary data to this article can be found online at http://dx.doi.org/10.1016/j.bbabio.2014.02.006.

Acknowledgement

We thank Bruno M. Fonseca for helpful discussions and together with Isabel Pacheco for the help in the purification of both proteins.

This work was supported by Fundação para a Ciência e a Tecnologia (FCT) — Portugal (Grants REEQ/336/BIO/2005, PEst-OE/EQB/LA0004/2011, PTDC/BIA-PRO/117523/2010 and SFRH/BPD/34591/2007 (to C.M.P.)). The NMR experiments were performed at the National NMR Facility supported by FCT (RECI/BBB-BQB/0230/2012).

References

[1] R. Baradaran, J.M. Berrisford, G.S. Minhas, L.A. Sazanov, Crystal structure of the entire respiratory complex I, Nature 494 (2013) 443–448.
[2] T.M. Iverson, C. Luna-Chavez, G. Cecchini, D.C. Rees, Structure of the *Escherichia coli* fumarate reductase respiratory complex, Science 284 (80) (1999) 1961–1966.
[3] J.C. Fontecilla-Camps, A. Volbeda, C. Cavazza, Y. Nicolet, Structure/function relationships of [NiFe]- and [FeFe]-hydrogenases, Chem. Rev. 107 (2007) 4273–4303.
[4] E.T. Judd, M. Youngblut, a.A. Pacheco, S.J. Elliott, Direct electrochemistry of *Shewanella oneidensis* cytochrome *c* nitrite reductase: evidence of interactions across the dimeric interface, Biochemistry (2012) 10175–10185.
[5] E. Rothery, C.G. Mowat, C.S. Miles, M.D. Walkinshaw, G.A. Reid, S.K. Chapman, Histidine 61: an important heme ligand in the soluble fumarate reductase from *Shewanella frigidimarina*, Biochemistry 42 (2003) 13160–13169.
[6] S. Dementin, B. Burlat, V. Fourmond, F. Leroux, P.-P. Liebgott, A. Abou Hamdan, C. Léger, M. Rousset, B. Guigliarelli, P. Bertrand, Rates of intra- and intermolecular electron transfers in hydrogenase deduced from steady-state activity measurements, J. Am. Chem. Soc. 133 (2011) 10211–10221.
[7] S.L. Pealing, A.C. Black, F.D.C. Manson, F.B. Ward, S.K. Chapman, G.A. Reid, Sequence of the gene encoding flavocytochrome, Biochemistry 31 (1992) 12132–12140.
[8] H. Gao, S. Barua, Y. Liang, L. Wu, Y. Dong, S. Reed, J. Chen, D. Culley, D. Kennedy, Y. Yang, Z. He, K.H. Nealson, J.K. Fredrickson, J.M. Tiedje, M. Romine, J. Zhou, Impacts of *Shewanella oneidensis* c-type cytochromes on aerobic and anaerobic respiration, Microb. Biotechnol. 3 (2010) 455–466.
[9] T.E. Meyer, A.I. Tsapin, I. Vandenberghe, L. de Smet, D. Frishman, K.H. Nealson, M.A. Cusanovich, J.J. van Beeumen, Identification of 42 possible cytochrome *c* genes in the *Shewanella oneidensis* genome and characterization of six soluble cytochromes, OMICS 8 (2004) 57–77.
[10] B. Schuetz, M. Schicklberger, A.M. Spormann, J. Gescher, J. Kuermann, Periplasmic electron transfer via the c-type cytochromes MtrA and FccA of *Shewanella oneidensis* MR-1, Appl. Environ. Microbiol. 75 (2009) 7789–7796.
[11] C.J. Jeffery, Moonlighting proteins, Trends Biochem. Sci. 24 (1999) 8–11.
[12] P. Taylor, S.L. Pealing, G.A. Reid, S.K. Chapman, M.D. Walkinshaw, Structural and mechanistic mapping of a unique fumarate reductase, Nat. Struct. Biol. 6 (1999) 1108–1112.
[13] D. Leys, A.S. Tsapin, K.H. Nealson, T.E. Meyer, M.A. Cusanovich, J.J. Van Beeumen, Structure and mechanism of the flavocytochrome *c* fumarate reductase of *Shewanella putrefaciens* MR-1, Nat. Struct. Biol. 6 (1999) 1113–1118.
[14] M. Doherty, S.L. Pealing, C.S. Miles, R. Moysey, P. Taylor, M.D. Walkinshaw, G.A. Reid, S.K. Chapman, Identification of the active site acid/base catalyst in a bacterial fumarate reductase: a kinetic and crystallographic study, Biochemistry (2000) 10695–10701.
[15] M. Pessanha, E. Rothery, C.S. Miles, G. a Reid, S.K. Chapman, R.O. Louro, D.L. Turner, C. a Salgueiro, A.V. Xavier, Tuning of functional heme reduction potentials in *Shewanella fumarate* reductases, Biochim. Biophys. Acta 1787 (2009) 113–120.
[16] B.M. Fonseca, C.M. Paquete, S.E. Neto, I. Pacheco, C.M. Soares, R.O. Louro, Mind the gap: cytochrome interactions reveal electron pathways across the periplasm of *Shewanella oneidensis* MR-1, Biochem. J. 108 (2013) 101–108.
[17] S.L. Pealing, M.R. Cheesman, G.A. Reid, A.J. Thomson, F.B. Ward, S.K. Chapman, Spectroscopic and kinetic studies of the tetraheme flavocytochrome *c* from *Shewanella putrefaciens* NCIMB400, Biochemistry 34 (1995) 6153–6158.
[18] M. Husain, V. Massey, Reversible resolution of flavoproteins into apoproteins and fee flavins, Methods Enzymol. 53 (1978) 429–437.
[19] P. Macheroux, UV–visible spectroscopy as a tool to study flavoproteins, Methods Mol. Biol. 131 (1999) 1–7.

[20] T. Catarino, D.L. Turner, Thermodynamic control of electron transfer rates in multicentre redox proteins, Chembiochem 2 (2001) 416–424.
[21] C.M. Paquete, D.L. Turner, R.O. Louro, A.V. Xavier, T. Catarino, Thermodynamic and kinetic characterisation of individual haems in multicentre cytochromes c_3, Biochim. Biophys. Acta 1767 (2007) 1169–1179.
[22] M. Dixon, The acceptor specificity of flavins and flavoproteins. I. Techniques for anaerobic spectrophotometry, Biochim. Biophys. Acta 226 (1971) 241–258.
[23] D.O. Lambeth, G. Palmer, The kinetics and mechanism of reduction of electron transfer proteins and other compounds of biological interest by dithionite, J. Biol. Chem. 248 (1973) 6095–6103.
[24] K.L. Pankhurst, C.G. Mowat, E. Rothery, J.M. Hudson, A.K. Jones, C.S. Miles, M.D. Walkinshaw, F.A. Armstrong, G.A. Reid, S.K. Chapman, A proton delivery pathway in the soluble fumarate reductase from *Shewanella frigidimarina*, J. Biol. Chem. 281 (2006) 20589–20597.
[25] R.A. Marcus, N. Sutin, Electron transfers in chemistry and biology, Biochim. Biophys. Acta 811 (1985) 265–322.
[26] S.G. Mayhew, The redox potential of dithionite and SO-2 from equilibrium reactions with flavodoxins, methyl viologen and hydrogen plus hydrogenase, Eur. J. Biochem. 85 (1978) 535–547.
[27] H.E.M. Christensen, I. Coutinho, H. Jensen, S. Conrad, J.M. Hammerstad-Pedersen, J.J. Karlsson, J. Ulstrup, A.V. Xavier, Electron transport networks in multicentre metalloproteins, J. Photochem. Photobiol. A Chem. 82 (1994) 103–115.
[28] K. Turner, M. Doherty, H.A. Heering, F.A. Armstrong, G.A. Reid, S.K. Chapman, Redox properties of flavocytochrome c_3 from *Shewanella frigidimarina* NCIMB400, Biochemistry 38 (1999) 3302–3309.
[29] B.M. Fonseca, C.M. Paquete, C.A. Salgueiro, R.O. Louro, The role of intramolecular interactions in the functional control of multiheme cytochromes *c*, FEBS Lett. 586 (2012) 504–509.
[30] J.C. Lagarias, J.A. Reeds, M.H. Wright, P.E. Wright, Convergence properties of the Nelder—mead simplex method in low dimensions, SIAM J. Optim. 9 (1998) 112–147.
[31] L.J.C. Jeuken, A.K. Jones, S.K. Chapman, G. Cecchini, F.A. Armstrong, Electron-transfer mechanisms through biological redox chains in multicenter enzymes, J. Am. Chem. Soc. 124 (2002) 5702–5713.
[32] A.K. Jones, R. Camba, G.A. Reid, S.K. Chapman, F.A. Armstrong, Interruption and time-resolution of catalysis by a flavoenzyme using fast scan protein film voltammetry, J. Am. Chem. Soc. 122 (2000) 6494–6495.
[33] E. Rothery, C.G. Mowat, C.S. Miles, S. Mott, M.D. Walkinshaw, G.A. Reid, S.K. Chapman, Probing domain mobility in a flavocytochrome, Biochemistry 43 (2004) 4983–4989.
[34] A. Abou Hamdan, S. Dementin, P.-P. Liebgott, O. Gutierrez-Sanz, P. Richaud, A.L. De Lacey, M. Rousset, P. Bertrand, L. Cournac, C. Léger, Understanding and tuning the catalytic bias of hydrogenase, J. Am. Chem. Soc. 134 (2012) 8368–8371.
[35] V. Fourmond, C. Baffert, K. Sybirna, T. Lautier, A. Abou Hamdan, S. Dementin, P. Soucaille, I. Meynial-Salles, H. Bottin, C. Léger, Steady-state catalytic wave-shapes for 2-electron reversible electrocatalysts and enzymes, J. Am. Chem. Soc. 135 (2013) 3926–3938.
[36] A.S. Beliaev, D.K. Thompson, T. Khare, H. Lim, C.C. Brandt, G. Li, A.E. Murray, J.F. Heidelberg, C.S. Giometti, J. Yates, K.H. Nealson, J.M. Tiedje, J. Zhoui, Gene and protein expression profiles of *Shewanella oneidensis* during anaerobic growth with different electron acceptors, OMICS 6 (2002) 39–60.